

Article

Hydrogen Production System Using Alkaline Water Electrolysis Adapting to Fast Fluctuating Photovoltaic Power

Xing Cao ¹, Jingang Wang ^{1,*}, Pengcheng Zhao ¹, Haiting Xia ¹, Yun Li ², Liming Sun ² and Wei He ¹

¹ State Key Laboratory of Power Transmission Equipment and System Security and New Technology, Chongqing University, Chongqing 400044, China; 202011021036@cqu.edu.cn (X.C.); zhaopengcheng@cqu.edu.cn (P.Z.); 20211101037@cqu.edu.cn (H.X.); hewei@cqu.edu.cn (W.H.)

² Chongqing Yuxin Pingrui Electronic Co., Ltd., Chongqing 401329, China; yunli_yuxin@sina.com (Y.L.); lm_sun_yx@sina.com (L.S.)

* Correspondence: jingang_023@163.com

Abstract: Using photovoltaic (PV) energy to produce hydrogen through water electrolysis is an environmentally friendly approach that results in no contamination, making hydrogen a completely clean energy source. Alkaline water electrolysis (AWE) is an excellent method of hydrogen production due to its long service life, low cost, and high reliability. However, the fast fluctuations of photovoltaic power cannot integrate well with alkaline water electrolyzers. As a solution to the issues caused by the fluctuating power, a hydrogen production system comprising a photovoltaic array, a battery, and an alkaline electrolyzer, along with an electrical control strategy and energy management strategy is proposed. The energy management strategy takes into account the predicted PV power for the upcoming hour and determines the power flow accordingly. By analyzing the characteristics of PV panels and alkaline water electrolyzers and imposing the proposed strategy, this system offers an effective means of producing hydrogen while minimizing energy consumption and reducing damage to the electrolyzer. The proposed strategy has been validated under various scenarios through simulations. In addition, the system's robustness was demonstrated by its ability to perform well despite inaccuracies in the predicted PV power.

Keywords: photovoltaic energy system; water electrolyzer; energy management; renewable energy



Citation: Cao, X.; Wang, J.; Zhao, P.; Xia, H.; Li, Y.; Sun, L.; He, W.

Hydrogen Production System Using Alkaline Water Electrolysis Adapting to Fast Fluctuating Photovoltaic Power. *Energies* **2023**, *16*, 3308.

<https://doi.org/10.3390/en16083308>

Academic Editor: Samuel Simon Araya

Received: 11 March 2023

Revised: 28 March 2023

Accepted: 30 March 2023

Published: 7 April 2023



Copyright: © 2023 by the authors. Licensee MDPI, Basel, Switzerland. This article is an open access article distributed under the terms and conditions of the Creative Commons Attribution (CC BY) license (<https://creativecommons.org/licenses/by/4.0/>).

1. Introduction

Environmental protection has become a widely accepted concept, leading to an urgent need for clean energy transfer. Hydrogen, which has a high specific energy density and only produces water, is a promising alternative to fossil fuels [1–3]. However, to ensure sustainability, it is essential to produce hydrogen through a clean process. One effective method is to use renewable energy, such as solar power, for water electrolysis, which does not produce any contamination or carbon emissions [4–7]. On the other hand, hydrogen production through water electrolysis is a sustainable and promising approach to store excess electricity from intermittent renewable energy sources [8]. There are three primary methods for water electrolysis, including alkaline water electrolysis, proton exchange membrane water electrolysis, and solid oxide water electrolysis [9,10]. The most widely used method is alkaline water electrolysis using an alkaline electrolyzer, which has the advantages of long service life, low cost, and high reliability [11–14]. However, due to the slow mass transfer and electrochemical reaction, the alkaline water electrolyzer is unable to accommodate fluctuating PV energy, which can damage the electrolyzer and increase energy consumption [15]. Fluctuating PV energy also leads to a high number of startup and shutdown cycles, which can cause degradation of nickel electrodes, exceed the maximum start/stop count, and reduce the expected system lifetime. The electrolyzer cannot operate when the hydrogen production capacity drops below 25%, because the percentage of hydrogen transferred to the oxygen flow increases significantly, which may

have a risk of explosion [16]. Frequent startup and shutdown also create an imbalanced pressure between hydrogen and oxygen, which can lead to the mixing of the two and cause gas impurities [17]. Moreover, Huang P et al. found that the gas purity in AWE can also be affected by mixing the anodic and cathodic electrolyte cycles due to intermittent power supply, which transports dissolved electrolysis products into opposite half-cell compartments [18]. Additionally, with fluctuations in input power, the gas production volume of hydrogen and oxygen on both sides of the electrolyzer fluctuates, resulting in changes to the liquid level on both sides of the electrolyzer. This requires frequent operation of the liquid level balance device, thereby shortening the service life of pneumatic or solenoid valves, increasing the consumption of auxiliary machines, and reducing the comprehensive electrolysis efficiency [19]. To address the limitations of current electrolyzers to the fluctuating renewable power input, from theoretical analysis to engineering practice, various approaches have been proposed, including the development of new designs and control strategies.

Many researchers analyzing this phenomenon theoretically. Shen et al. created a mathematical model for an alkaline water electrolyzer, revealing that electrolytic voltage and current is in relation to electrolyte temperature and system pressure [20]. Zhu et al. investigated the interaction between mass transfer, electrochemical reaction, and bubble effect, aiming to develop electrolyzers that are compatible with fluctuating renewable power sources; they found that the bubble-driven convection was more predominated. [21]. Balabel et al. demonstrated that the efficiency of hydrogen production by AWE is influenced by different operating and geometrical parameters, as well as hydrogen bubble generation. They identified optimal conditions for electrolysis, which can be achieved through specific input voltage, electrode gap distance, and solution concentration, and found that an empirical correlation can be used to predict the optimum operating conditions from the performance curves of the alkaline water electrolyzer [22]. Despite the mechanism analysis of the electrolyzer, others focused on the control strategy of the electrolyzer. Bergen et al. analyzed the response of the electrolyzer to renewable sources, and observed a reduction of hydrogen production during the transient process, finding that maintain a minimal current of 10 A after the sudden shutdown will greatly reduce the performance loss caused by the dynamic event, which introduces another constraint on the common operating strategy for renewable energy systems [23]. Ursúa A et al. proposed two strategies for enhancing the AWE operating under renewable energy, namely allowing the electrolyzer to function for 10 min under the lower operating limit and integrating a battery bank, which can reduce the number of stops by up to 62.1% [24]. However, this does not take the effect of current efficiency into consideration, make it cost more when the electrolyzer operates under the lower operating limit.

The integration of alkaline water electrolyzers with fluctuating photovoltaic power has been a persistent problem in the field of absorbing renewable energy by water electrolysis. In order to address this issue, this study has been undertaken with the aim of proposing an easy-to-apply method that can effectively eliminate power fluctuations and optimize the usage of photovoltaic energy. This study provides a resolution by utilizing an alkaline electrolyzer, a PV array, a battery pack, and corresponding controllers. To begin with, the system was carefully engineered to ensure compatibility between the battery capacity, PV panel peak value, and the electrolyzer. Subsequently, the electrical control of the system was carefully devised to ensure optimal performance under different disturbances, providing a stable base for power flow control. The models of each component, particularly the electrolyzer, were constructed using actual measured data. Lastly, taking into account the characteristics of PV power and the electrolyzer, an energy management strategy was suggested that relies on PV power prediction, and this approach was demonstrated to be efficacious under diverse conditions. This study provides an easy and applicable resolution to stable hydrogen production under fast fluctuating PV energy considering the actual circumstances. By developing a reliable and efficient method for reducing power fluctuations for the electrolyzer, this study is able to promote the wider adoption of

renewable energy technologies and to support the transition towards a more sustainable and environmentally friendly energy future.

2. System Design and Modeling

2.1. System Components

The system diagram is presented in Figure 1, showcasing the main components, which include a 6.7 kWp PV array, a 6 kW battery pack, and an alkaline electrolyzer with an operating range of 2 kW to 5.8 kW. The battery can solely support one-hour operation of the electrolyzer, which could greatly enhance the robustness of the system. The peak power of the photovoltaic array is near the maximum operating power of the electrolyzer, which will not cause a waste of energy. The PV power output is greatly affected by varying radiation and temperatures; hence, to maximize the utilization of solar energy, the maximum power point tracking (MPPT) algorithm is employed [25–27]. The duty cycle of the PV converter is controlled by the MPPT algorithm to achieve the maximum available power at any given time. In order to regulate the voltage of the DC bus, the dual closed-loop control strategy is implemented to control the bidirectional DC/DC converter. The control system compares the current bus voltage with the reference value, calculates the voltage difference, and then controls the converter to either charge or discharge the battery based on the voltage difference to maintain the bus voltage within the desired range. The AWE is connected to the microgrid through a buck converter, and the duty cycle of this converter is adjusted according to the modified input power of the electrolyzer.

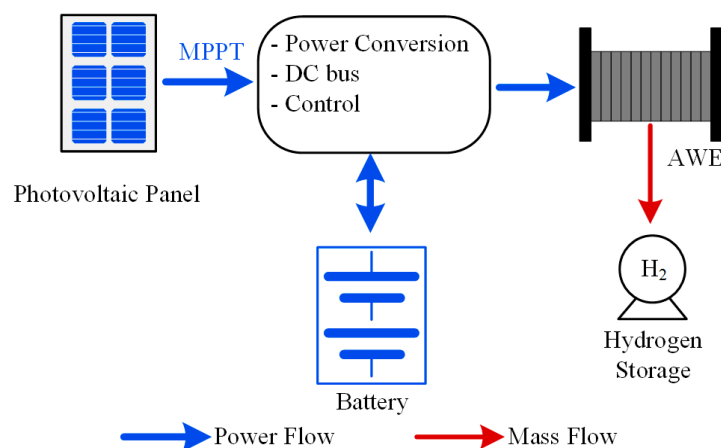


Figure 1. Schematic representation of the system.

2.2. Model of the PV Panel and Its Control Design

The output electrical characteristics of the PV array at 25 °C are shown in Figure 2. As the curves indicate, the output power of the PV array changes with the level of radiation. For a specific radiation and temperature, the output power only depends on the voltage, and the curve follows a single-peak shape. Therefore, the voltage of the PV array can be adjusted to track the maximum power point (MPP). However, due to the intermittent nature of radiation, the MPP varies with time and can cause significant power losses if not tracked promptly. To address this, an adaptive maximum power point tracking algorithm using perturb and observation is employed to maximize PV power. The algorithm detects whether the operating point voltage exceeds the MPP voltage by analyzing changes in power and voltage and adjusts the voltage accordingly towards the MPP. It can be obtained from the power versus voltage curve; if the voltage is smaller than that of MPP, the output power will increase as the voltage rises, and if the voltage exceeds the voltage of MPP, the output power will decrease as the voltage rises. The procedure of this adaptive MPPT algorithm using this characteristic is shown in Figure 3. The D , which is the duty cycle of the boost converter controller, is used to control the output voltage. Since dP/dU becomes more

prominent as the operating point approaches the MPP, ΔD is modified by the exponential term of dP/dU so that the voltage would not oscillate around the MPP.

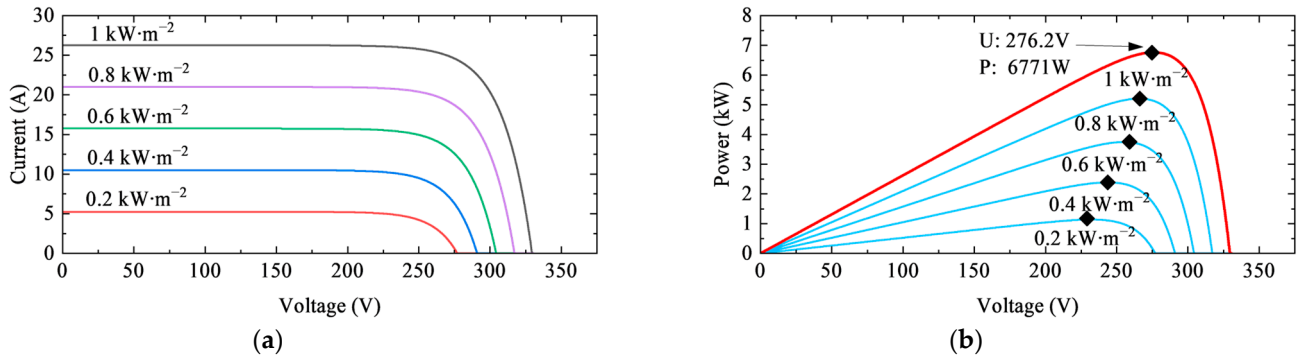


Figure 2. Electrical characteristics of PV array at 25 °C. (a) Current versus voltage curve under different radiation; (b) power versus voltage curve under different radiation.

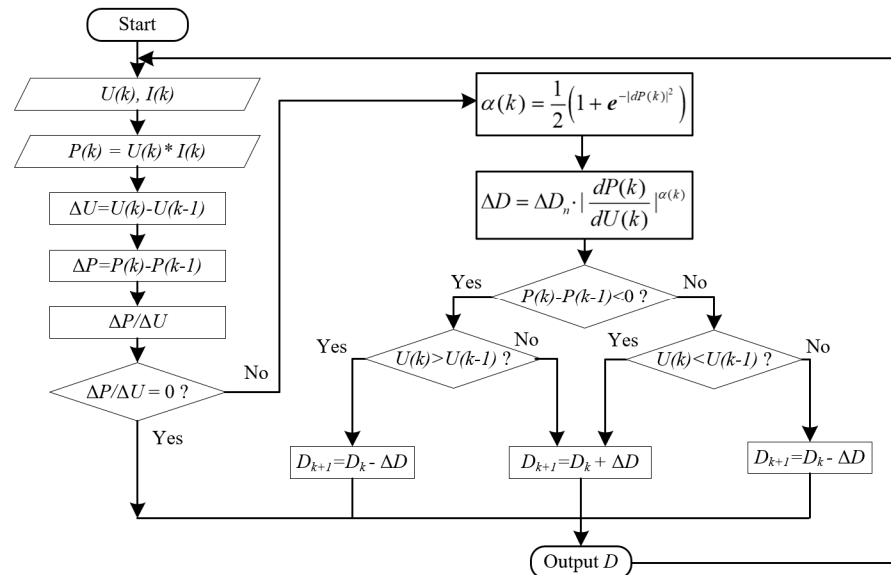


Figure 3. Procedure of adaptive MPPT algorithm.

By analyzing the power versus voltage curve, it can be observed that when the voltage is below the MPP, the output power increases as the voltage rises, but when the voltage exceeds the MPP, the output power decreases as the voltage increases. Thus, the adaptive MPPT algorithm presented in Figure 3 utilizes this characteristic. The duty cycle of the boost converter controller, denoted as D , is used to regulate the output voltage. As the operating point approaches the MPP, dP/dU becomes more significant, and hence, the modification of ΔD is determined by the exponential term of dP/dU , ensuring that the voltage does not oscillate around the MPP.

2.3. Mathematical Model of Alkaline Electrolyzer

The alkaline electrolyzer comprised multiple cells connected in series and filled with electrolytes, with hydrogen and oxygen being generated from the electrodes on either side. Aqueous potassium hydroxide (KOH) has been commonly used as the electrolyte in conventional alkaline electrolyzers, with solutions of 20–30 wt% due to their high conductivity in this concentration range. Typically, these electrolyzers operate at temperatures between 80 and 90 degrees Celsius and pressures of 8–16 bar.

Several models have been proposed to capture the U-I characteristic of an alkaline water electrolyzer under varying conditions [28,29]. These models primarily focus on the three factors that contribute to cell voltage—reversible cell voltage, ohmic losses, and activation

overvoltage—which are dependent on various parameters such as electrolyte concentration, operating temperature, current density, and pressure. Therefore, the proposed models aim to accurately represent these factors under different conditions.

Formula (1) considers the operation temperature T and the current density j . While the parameters r_i reflects ohmic losses, s and t_i stand for the activation overvoltage of the oxygen and hydrogen evolution reactions; U_{cel} is the average cell value. All parameters can be derived from measured data [30–33].

$$U_{cel} = U_{rev} + (r_1 + r_2 \cdot T) \cdot j + s \cdot \log_1 \left[\left(t_1 + \frac{t_2}{T} + \frac{t_3}{T^2} \right) \cdot j + 1 \right] \quad (1)$$

where:

$$U_{rev} = U_{rev0} + \frac{R(273.15 + T)}{zF} \ln \left(\frac{p}{p_0} \right) \quad (2)$$

$U_{rev0} = 1.229$ V is the reversible voltage at standard conditions, thus p_0 (101 kPa) is the ambient pressure. $z = 2$ is the number of exchanged electrons, R is the universal gas constant, and $F(96,485 \text{ C} \cdot \text{mol}^{-1})$ is the Faraday constant. p is the current operating pressure, which is constant at 13 bar in this study. Equation (1) is empirical and therefore differs in different systems.

To develop a model for an alkaline water electrolyzer, an experiment was performed using an industrial electrolyzer comprising 12 cells in series. The electrolyzer has a nominal voltage of 24 V and a rated current of 220 A, with a crossover section area of 0.062 m², and an operating power range of 2 kW to 5.8 kW. The U-I curve of the electrolyzer was measured independently at different electrolyte temperatures ranging from 60 to 85 °C to derive the temperature-independent parameter s ; the operating pressure is set to be constant at 1.3 MPa during the system operating. Furthermore, curve fitting was employed to obtain the temperature-dependent parameters r and t , and their respective values are listed in Table 1. The model of the electrolyzer is based on the assumption that the operating pressure remains constant throughout its operation, and that the cooling device can promptly respond to maintain the temperature within a narrow range.

Table 1. Parameters of the electrolyzer model.

Parameter	Value
r_1	9.7×10^{-5}
r_2	-2.7×10^{-7}
s	0.086
t_1	0.0032
t_2	-25
t_3	2600
A	0.062 m ²

Figure 4a displays the measured data and corresponding fitted curve at 85 °C. Due to the variation in temperature during operation and the time it takes for the reaction to establish chemical equilibrium, the voltametric characteristic may not be entirely accurate. However, the actual circumstance aligned with the results at all available operating points, which validates the findings.

Despite the voltametric characteristic of the electrolyzer, the hydrogen production characteristic needs to be identified. In addition, to precisely calculate the real amount of hydrogen production, the effect of current efficiency must be taken into account. Equation (3) is an empirical expression that depicts the current efficiency for a given temperature, which shows that the current efficiency is only current dependent under certain situations [29].

$$\eta_F = f_1 \frac{j^2}{f_2 + j^2} \quad (3)$$

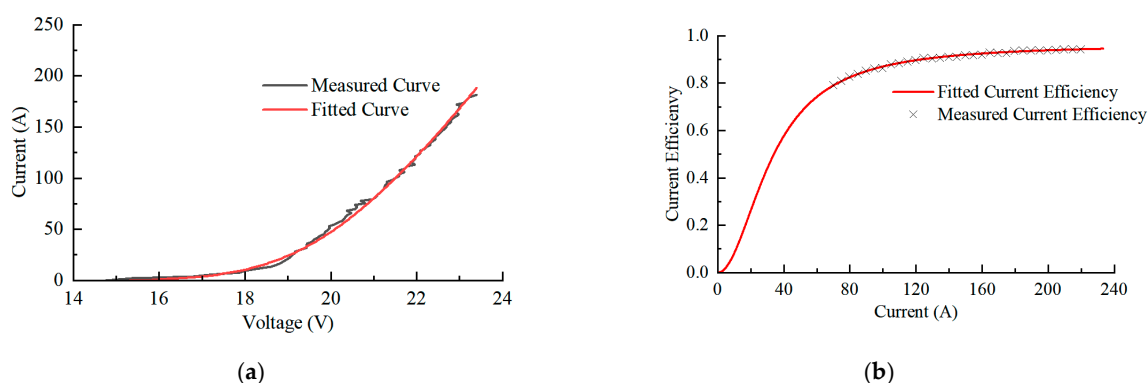


Figure 4. Electrical and current efficiency characteristics of the electrolyzer. (a) Voltametric curve of the electrolyzer at 85 °C; (b) current efficiency of the electrolyzer under different current at 85 °C.

To obtain the actual current efficiency under various current densities, the temperature is set to be 85 °C and varies only a little which can be ignored. The electrolyzer operates at constant-current mode from 70 A to 230 A in a step of 5 A, and it operates for half an hour at each current level; thus, the current efficiency is obtained from the actual amount of hydrogen produced and the theoretical value. In order to avoid the fluctuation of hydrogen production caused by current adjustment from affecting the accuracy of current efficiency, it takes 5 min each time before starting to record the hydrogen production.

Figure 4b shows the current efficiency of the electrolyzer at 85 °C, the crossed dots are measured current efficiency and the red curve is the fitted value of the current efficiency. The parameters f_1 and f_2 in Equation (3) are 0.9622 and 379,200, respectively. The hydrogen production can be calculated using Formula (4):

$$H_P = 4.18 \times 10^{-4} \eta_F n I_{ele} t \tag{4}$$

where H_P is the hydrogen production in Nm^3 ; η_F is the current efficiency; n is the number of electrolyzer cells; I_{ele} is the operating current in amperes; and t is the operating time in hours. Due to the nonlinearity of the current efficiency and voltametric characteristics of the electrolyzer, the electrolyzer has a certain operating region that can achieve the best energy consumption performance. The result obtained from Equations (1) and (3) is plotted in Figure 5a. The convex shape of the energy consumption curve indicates that the electrolyzer’s best performance was achieved when it operates at a medium power level. Therefore, the energy management strategy should aim to maintain the electrolyzer’s operation in this range as frequently as possible. While in the rated current (220 A), the energy consumption of $5.26 \text{ kWh}\cdot Nm^{-3}$ was not the most efficient performance, but it is still acceptable to prioritize a higher hydrogen production rate even if it comes at the cost of increased energy consumption.

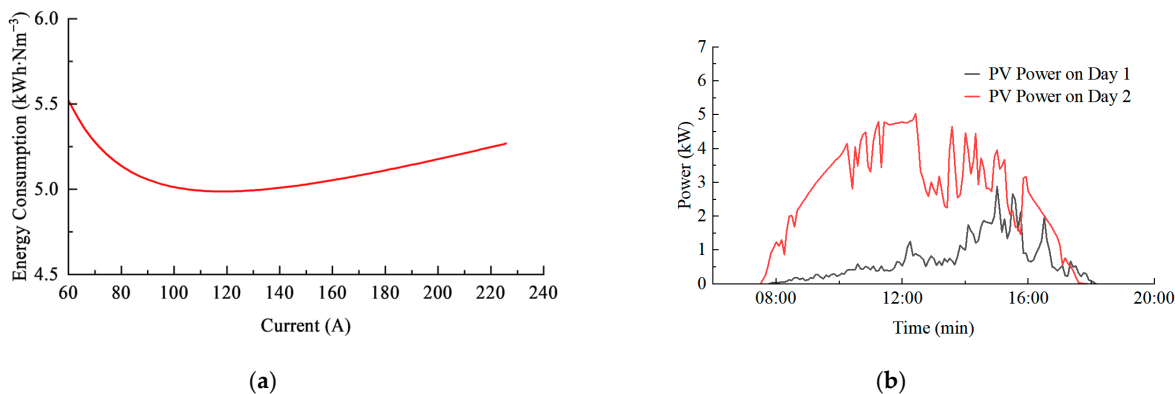


Figure 5. (a) Energy consumption under different current density; (b) different PV power on different days.

3. Energy Management Design

The energy management strategy developed for the system takes into consideration not only the characteristics of the electrolyzer but also those of the PV power. The PV power exhibits significant variation as the time changes, as is shown in Figure 5b. Such large fluctuations make it difficult to implement a conventional control strategy. However, there is a general tendency for the output power to increase from morning to noon and decrease from afternoon to night. Based on this observation, an energy management strategy is proposed. The capacity of the electrolyzer, battery, and peak value of the PV array are carefully designed to suit the system.

After building the system, the energy management strategy is presented in Figure 6, where the electrolyzer power is determined based on the current SOC of the battery, as well as the average predicted power of the next half hour (P_{r30}) and next hour (P_{r60}). The decision to not consider further prediction of PV power is due to the reduced accuracy of such predictions as the prediction horizons expand. The electrolyzer power is adjusted every 5 min, providing sufficient time for it to reach a steady state. The goal of this strategy is to utilize the battery’s capacity to mitigate the fluctuation of the power supplied to the electrolyzer and ensure it operates in a high-efficiency power interval. To achieve this, the tendency of PV power change is taken into consideration, and the corresponding power management approach is adopted.

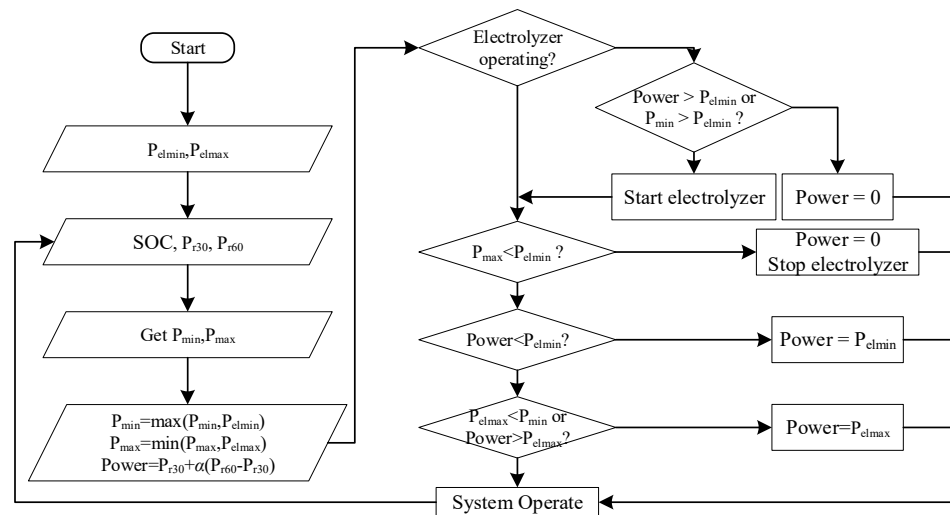


Figure 6. Energy management strategy of the hydrogen production system.

Firstly, set the minimal and maximum electrolyzer power P_{elmin} and P_{elmax} , respectively. Then, during the operating process, obtain the current status of the system, including current battery SOC and use the predicted power P_{r30} to get the maximum and minimal available power P_{max} and P_{min} , for the next half an hour. This aims to avoid the battery overcharge or over discharge, and reduce sudden power increase or drop considering the battery SOC; this time interval considers both the prediction accuracy and the performance of control strategy.

$$\begin{aligned}
 P_{max} &= P_{r30} + 2(SOC - 0.2)W_b \\
 P_{min} &= P_{r30} + 2(0.9 - SOC)W_b
 \end{aligned}
 \tag{5}$$

where the W_b denotes the maximum energy capacity of the battery. The P_{min} and P_{max} considers the maximum charge and discharge capacity of the battery and thus provide a rather large range of operating power for the electrolyzer. To simplify the control, the dynamic behavior of the battery is not taken into consideration.

Secondly, make sure the P_{min} and P_{max} are in normal range and get the power of the electrolyzer. Because the curve of the energy consumption versus current is convex, the tendency of the PV power change is considered in the calculation to ensure that the electrolyzer power remains within the optimal range. Specifically, the electrolyzer power is

increased earlier when the predicted PV power is expected to decrease, and vice versa. This approach helps to prevent the electrolyzer power from being too high or too low, which can lead to inefficiencies and decreased performance. Thus, the electrolyzer power is set to be

$$Power = P_{r30} + \alpha(P_{r60} - P_{r30}) \quad (6)$$

The parameter α is a function of the SOC and is used to maintain steady-state operation of the electrolyzer. When the SOC is high, α is set to a higher value, releasing the energy it stores to ensure that the electrolyzer operates at a steady-state power level later. Conversely, when the SOC is low, α is set to a lower value to reduce the electrolyzer's power and prevent the battery from being depleted due to lack of power. To avoid frequent startups and shutdowns of the electrolyzer, a hysteresis characteristic is implemented to control the electrolyzer's on/off status switch. The electrolyzer is started when the system has sufficient power and stopped when the system lacks energy.

Finally, the limitation of the electrolyzer power must be also taken into consideration. If the maximum power (P_{max}) of the system is lower than the minimum power (P_{elmin}) required by the electrolyzer, the electrolyzer power is set to zero to prevent the system from operating below its minimum required power level. Conversely, if the minimum power (P_{min}) of the system is higher than the maximum power (P_{elmax}) required by the electrolyzer, excess energy is discarded as the electrolyzer cannot consume it. This helps to ensure that the system operates within safe and optimal power levels, while also minimizing energy waste.

4. Results and Discussion

To validate the effectiveness of the proposed system topology and control strategy, a simulation of the system was conducted. Initially, the bus voltage and PV power waveforms were simulated under various disturbances to ensure the system's ability to operate consistently. Subsequently, the energy management strategy based on PV power prediction was executed to obtain the system's power flow and verify the proposed strategy's efficiency. The simulation results show that the proposed system topology and control strategy can operate effectively and achieve the expected performance under various operating conditions.

The electrical control strategy of the proposed system is illustrated in Figure 7a, which consists of three controllers. The MPPT controller regulates the boost converter to achieve maximum PV power utilization. The battery controller maintains the bus voltage at 400 volts by either charging or discharging the battery. Finally, the electrolyzer controller ensures that the electrolyzer power remains at the desired level. Each controller has been designed to work cohesively, contributing to the system's overall performance and efficiency.

Figure 7b illustrates the response of the system controllers in Figure 7a. When the radiance dropped from $1000 \text{ W}\cdot\text{m}^{-2}$ to $700 \text{ W}\cdot\text{m}^{-2}$, the controller was able to instantly adjust and attain the maximum power within just 0.01 s. Moreover, the transition process was even faster when the radiance dropped from $700 \text{ W}\cdot\text{m}^{-2}$ to $600 \text{ W}\cdot\text{m}^{-2}$, highlighting the efficacy of the MPPT controller. While the battery had a slower response time compared to the PV power, causing the bus voltage to drop by 6.25% from 400 Volts to 375 Volts, it was still within a tolerable time duration of 0.03 s. Since the system can operate normally and achieve maximum PV power input despite radiance disturbances, the employed energy management strategy could be used to minimize the damage caused by fluctuations during electrolysis. The results demonstrate the capability of the proposed system topology and control strategy to handle disturbances effectively and maintain the system's overall performance.

With the effectiveness of the electrical control strategy now validated, we can shift our focus to the system control strategy for energy management. Figure 8 depicts the operational status on two separate days using this energy management strategy. The two days exhibited different irradiance levels, showcasing the applicability of the proposed

approach under various operating conditions. On day 1, the PV power was initially low, and the whole PV energy of the day was only 7.5 kWh. However, the battery gradually accumulated enough energy to sustain the electrolyzer. Despite the low PV power, the electrolyzer continued to operate at a low power level without any interruptions. The total energy absorbed by the electrolyzer was 8.68 kWh, resulting in the production of 1.68 Nm³ hydrogen, with an average energy consumption of 5.167 kWh·Nm⁻³. In addition, the electrolyzer operated at a rather stable mode, the electrolyzer power remained constant. However, as the battery power is the primary power source for the electrolyzer, it underwent a higher battery cycle, with its SOC ranging from 0.9 to 0.32.

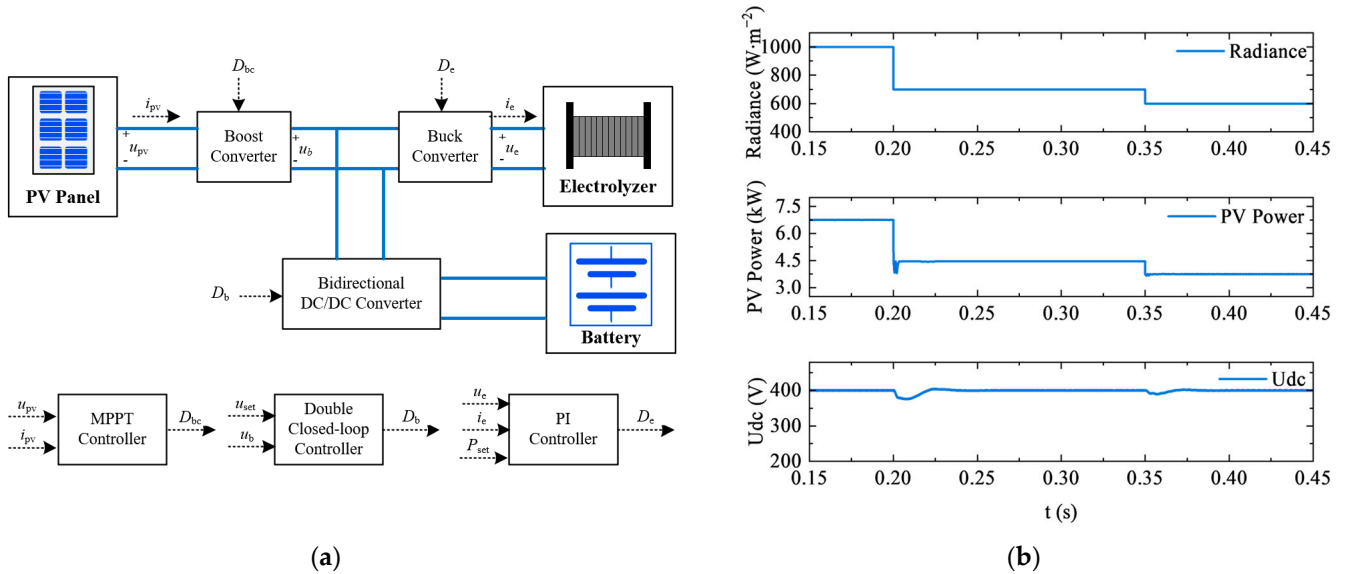


Figure 7. System electrical control strategy and its result. (a) The electrical control strategy for each component; (b) the system response under radiation disturbances.

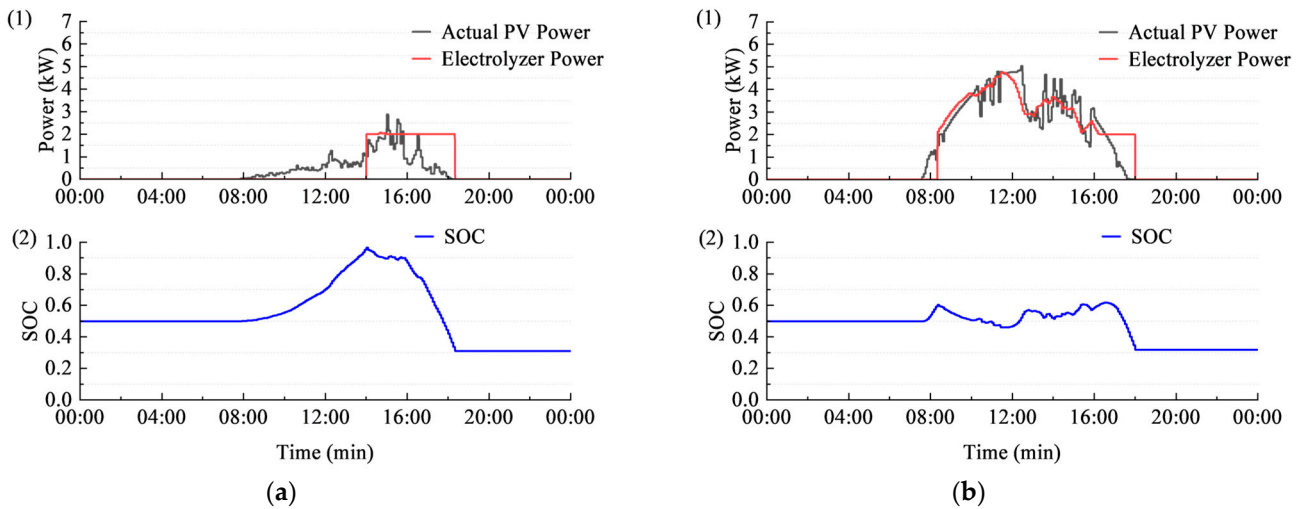


Figure 8. System operation status including actual PV power, electrolyzer power in (1), and SOC of the day using proposed energy management strategy in (2). (a) Operation status on day 1 with insufficient PV power; (b) operation status on day 2 with sufficient PV power.

The situation was quite different on day 2, the irradiance was adequate and still fluctuated significantly, resulting in a fluctuating PV power. At around 12:30, the PV power dropped from 5.03 kW to 2.59 kW rapidly; before the PV power started to drop, the electrolyzer power slowly dropped from 4.75 kW to 2.8 kW, which ensured the stable operation of the electrolyzer. In general, the electrolyzer power followed the fluctuating

power pattern but became smoother, resulting in a relatively consistent operating state for the system. While the electrolyzer was in operation, the PV power variation was 1.66, whereas the electrolyzer power variation was only 0.72, indicating the successful reduction of power fluctuations. Towards the end of the day, the energy stored in the battery was utilized to sustain the system's continuous operation. It took 30.26 kWh energy for the electrolyzer to produce hydrogen. In total, 5.997 Nm³ of hydrogen was produced, with an energy consumption rate of 5.046 kWh·Nm⁻³, which is near optimal. Furthermore, when compared to day 1, the battery SOC was within a narrower range from 0.3 to 0.6 which is beneficial for extending the lifespan of the battery.

The effectiveness of the control strategy has been verified, but in fact, there were errors in the prediction of photovoltaic power generation, and thus it is important to consider the accuracy of the predicted PV power. We used the hybrid neural network for PV power prediction, which takes the wind speed, temperature, relative humidity, global horizontal diffusion, and global titled radiation as inputs; the relative error of 90% prediction results was less than 7%. To account for this, a random noise was added to the predicted PV power to simulate its impact, and the noise followed a normal distribution with an average of 20% of current power. This is larger than the actual prediction error, so as to illustrate the performance of the control strategy. Although the real PV power was the same as that of day 2, there was a noticeable difference between the predicted and real PV power, as seen in Figure 9a. The larger fluctuations in the predicted PV power indicate a significant prediction error. The control strategy determines the power output of the electrolyzer, while the battery compensates for any surplus or deficit of solar energy. Despite this prediction error, the electrolyzer power remained stable and only experienced a slight change, as shown in Figure 9c. Compared with the result with no prediction error, the total hydrogen production from the electrolyzer was 5.990 Nm³, which is quite similar to the amount when there was no prediction error. From the comparison between Figures 8b and 9d, the main disadvantage caused by the prediction error is that the battery must undergo a larger discharge cycle due to the lower predicted PV power. This results in the battery storing surplus energy to prepare for potential shortages in PV power.

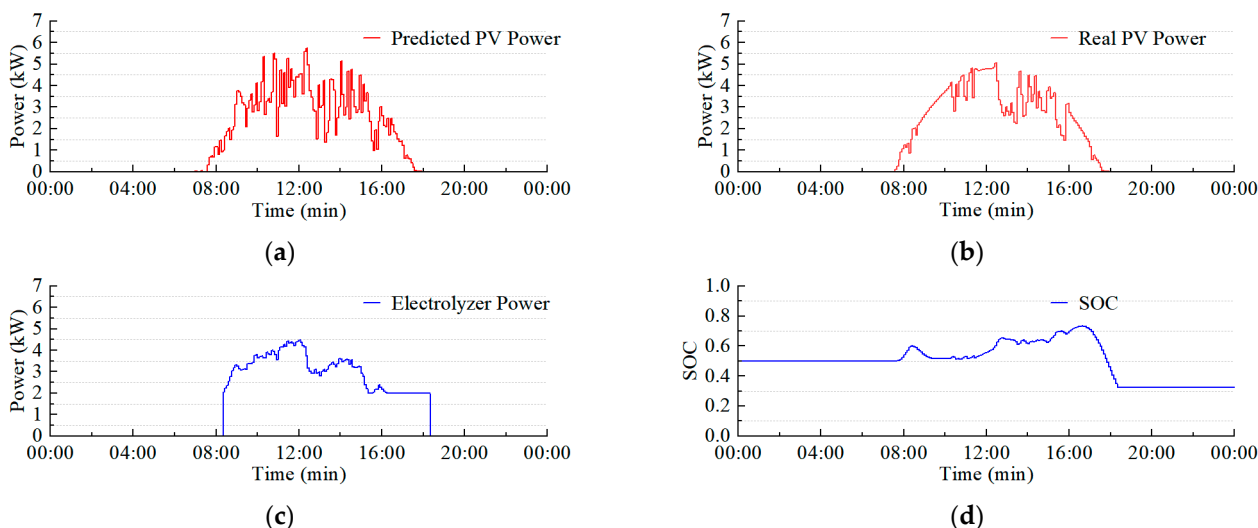


Figure 9. System status using proposed energy management strategy on day 2 with prediction error. (a) The predicted PV power; (b) the actual PV power on day 2; (c) the electrolyzer power during the day; (d) daily change of the battery SOC.

The proposed control strategy was confirmed to be effective based on the preceding discussion. By implementing this strategy, the power supplied to the electrolyzer experienced minimal fluctuations and only varied every 5 min. This duration is sufficient for the electrolyzer to attain a steady state and reduce any potential harm to the electrolyzer. Furthermore, the battery operated within a normal range, which could potentially extend

its lifespan. Additionally, its robustness was demonstrated by its successful operation in diverse scenarios and despite significant prediction errors.

5. Conclusions

Producing hydrogen through water electrolysis using PV power is considered a desirable way to generate green energy for the future. However, the integration of alkaline water electrolyzers with fast-fluctuating PV power has posed a challenge. To address this issue, a system comprising a PV panel, battery, and an alkaline water electrolyzer was developed. Moreover, the electrical characteristics of the newly developed system were meticulously taken into account, with particular emphasis on the alkaline water electrolyzer. Sufficient data was collected from a commercially available electrolyzer to construct a comprehensive mathematical model that includes its voltametric characteristics, power supply limitations, and energy consumption under various operating conditions. This model serves as a valuable tool for optimizing the performance of the system, ensuring its efficiency and sustainability.

Building upon the previous work, this paper implemented an electrical control and energy management strategy for the system. To maximize the PV power, the MPPT control algorithm was applied to the boost converter of the PV panel, allowing the system to respond instantaneously. Furthermore, an energy management strategy based on PV power prediction was proposed and proven to be effective. This strategy ensures that the system operates in a steady state by adjusting the power supplied to the electrolyzer every 5 min, providing sufficient time for the electrolyzer to reach chemical balance. Additionally, the PV power prediction enables power modifications in advance, allowing the electrolyzer to operate in a high-efficiency power range. Through simulations conducted on days with varying PV power and significant prediction errors, the effectiveness and robustness of the strategy were verified.

However, one major limitation of the proposed methods is that it requires the forecasting result of photovoltaic power, which can be challenging to obtain. Typically, this necessitates a lengthy and comprehensive record of photovoltaic power and meteorological parameters, rendering this approach unsuitable for some recently constructed systems. Furthermore, this method involves the use of batteries to mitigate fluctuations, which can increase the overall cost of the system. Future studies may consider the distribution of prediction errors and other electrical loads to enhance the performance of the system and reduce the capacity of the battery, to further increase its potential applications.

Author Contributions: Conceptualization, W.H. and J.W.; methodology, X.C.; software, X.C.; validation, X.C., P.Z. and H.X.; formal analysis, J.W., P.Z. and H.X.; investigation, X.C., P.Z. and H.X.; resources, Y.L. and L.S.; data curation, X.C.; writing—original draft preparation, X.C.; writing—review and editing, J.W.; visualization, J.W.; supervision, L.S.; project administration, Y.L.; funding acquisition, Y.L. All authors have read and agreed to the published version of the manuscript.

Funding: This research received no external funding.

Data Availability Statement: Data sharing is not applicable to this article.

Conflicts of Interest: The authors declare no conflict of interest.

Nomenclature

PV	Photovoltaic
AWE	Alkaline water electrolysis
MPP	Maximum power point
MPPT	Maximum power point tracking
SOC	State of charge
W_b	Maximum energy capacity of the battery
P_{r30}	Predicted average photovoltaic power of the next 30 min

P_{r60}	Predicted average photovoltaic power of the next 60 min
P_{elmin}	Minimal electrolyzer power
P_{elmax}	Maximum electrolyzer power
P_{min}	Minimal available power for the electrolyzer
P_{max}	Maximum available power for the electrolyzer

References

- Ehteshami, S.M.M.; Chan, S. The role of hydrogen and fuel cells to store renewable energy in the future energy network—Potentials and challenges. *Energy Policy* **2014**, *73*, 103–109. [[CrossRef](#)]
- Anderson, D.; Leach, M. Harvesting and redistributing renewable energy: On the role of gas and electricity grids to overcome intermittency through the generation and storage of hydrogen. *Energy Policy* **2004**, *32*, 1603–1614. [[CrossRef](#)]
- Luo, Z.; Hu, Y.; Xu, H.; Gao, D.; Li, W. Cost-Economic Analysis of Hydrogen for China's Fuel Cell Transportation Field. *Energies* **2020**, *13*, 6522. [[CrossRef](#)]
- Brauns, J.; Turek, T. Alkaline Water Electrolysis Powered by Renewable Energy: A Review. *Processes* **2020**, *8*, 248. [[CrossRef](#)]
- Hosseini, S.E.; Wahid, M.A. Hydrogen production from renewable and sustainable energy resources: Promising green energy carrier for clean development. *Renew. Sustain. Energy Rev.* **2016**, *57*, 850–866. [[CrossRef](#)]
- Mneimneh, F.; Ghazzawi, H.; Abu Hejjeh, M.; Manganelli, M.; Ramakrishna, S. Roadmap to Achieving Sustainable Development via Green Hydrogen. *Energies* **2023**, *16*, 1368. [[CrossRef](#)]
- Sarker, A.K.; Azad, A.K.; Rasul, M.G.; Doppalapudi, A.T. Prospect of Green Hydrogen Generation from Hybrid Renewable Energy Sources: A Review. *Energies* **2023**, *16*, 1556. [[CrossRef](#)]
- Bilodeau, A.; Agbossou, K. Control analysis of renewable energy system with hydrogen storage for residential applications. *J. Power Sources* **2006**, *162*, 757–764. [[CrossRef](#)]
- Chi, J.; Yu, H. Water electrolysis based on renewable energy for hydrogen production. *Chin. J. Catal.* **2018**, *39*, 390–394. [[CrossRef](#)]
- Nikolaïdis, P.; Poullikkas, A. A comparative overview of hydrogen production processes. *Renew. Sustain. Energy Rev.* **2017**, *67*, 597–611. [[CrossRef](#)]
- Yu, Z.; Duan, Y.; Feng, X.; Yu, X.; Gao, M.; Yu, S. Clean and Affordable Hydrogen Fuel from Alkaline Water Splitting: Past, Recent Progress, and Future Prospects. *Adv. Mater.* **2021**, *33*, e2007100. [[CrossRef](#)] [[PubMed](#)]
- Santos, D.M.F.; Sequeira, C.A.C.; Figueiredo, J.L. Hydrogen production by alkaline water electrolysis. *Quim. Nova* **2013**, *36*, 1176–1193. [[CrossRef](#)]
- David, M.; Ocampo-Martínez, C.; Sanchez-Pena, R. Advances in alkaline water electrolyzers: A review. *J. Energy Storage* **2019**, *23*, 392–403. [[CrossRef](#)]
- Marini, S.; Salvi, P.; Nelli, P.; Pesenti, R.; Villa, M.; Berrettoni, M.; Zangari, G.; Kiros, Y. Advanced alkaline water electrolysis. *Electrochimica Acta* **2012**, *82*, 384–391. [[CrossRef](#)]
- Sellami, M.; Loudiyi, K. Electrolytes behavior during hydrogen production by solar energy. *Renew. Sustain. Energy Rev.* **2017**, *70*, 1331–1335. [[CrossRef](#)]
- Ursúa, A.; Martín, I.S.; Barrios, E.L.; Sanchis, P. Stand-alone operation of an alkaline water electrolyser fed by wind and photovoltaic systems. *Int. J. Hydrogen Energy* **2013**, *38*, 14952–14967. [[CrossRef](#)]
- Mergel, J.; Stolten, D. Challenges in Water Electrolysis and Its Development Potential as a Key Technology for Renewable Energies. In *ECS Meeting Abstracts*; IOP Publishing: Bristol, UK, 2012; Volume MA2012-02, p. 348. [[CrossRef](#)]
- Haug, P.; Kreitz, B.; Koj, M.; Turek, T. Process modelling of an alkaline water electrolyzer. *Int. J. Hydrogen Energy* **2017**, *42*, 15689–15707. [[CrossRef](#)]
- Fang, R.; Liang, Y. Control strategy of electrolyzer in a wind-hydrogen system considering the constraints of switching times. *Int. J. Hydrogen Energy* **2019**, *44*, 25104–25111. [[CrossRef](#)]
- Shen, X.; Zhang, X.; Lie, T.T.; Li, G. Mathematical modeling and simulation for external electrothermal characteristics of an alkaline water electrolyzer. *Int. J. Energy Res.* **2018**, *42*, 3899–3914. [[CrossRef](#)]
- Zhu, J.; Zhang, X.; Lv, P.; Wang, Y.; Wang, J. An experimental investigation of convective mass transfer characterization in two configurations of electrolyzers. *Int. J. Hydrogen Energy* **2018**, *43*, 8632–8643. [[CrossRef](#)]
- Balabel, A.; Zaky, M.S.; Sakr, I. Optimum Operating Conditions for Alkaline Water Electrolysis Coupled with Solar PV Energy System. *Arab. J. Sci. Eng.* **2014**, *39*, 4211–4220. [[CrossRef](#)]
- Bergen, A.; Pitt, L.; Rowe, A.; Wild, P.; Djilali, N. Transient electrolyser response in a renewable-regenerative energy system. *Int. J. Hydrogen Energy* **2009**, *34*, 64–70. [[CrossRef](#)]
- Ursúa, A.; Barrios, E.L.; Pascual, J.; Martín, I.S.; Sanchis, P. Integration of commercial alkaline water electrolyzers with renewable energies: Limitations and improvements. *Int. J. Hydrogen Energy* **2016**, *41*, 12852–12861. [[CrossRef](#)]
- Ahmed, J.; Salam, Z. An Enhanced Adaptive P&O MPPT for Fast and Efficient Tracking Under Varying Environmental Conditions. *IEEE Trans. Sustain. Energy* **2018**, *9*, 1487–1496. [[CrossRef](#)]
- Murtaza, A.; Chiaberge, M.; Spertino, F.; Shami, U.T.; Boero, D.; De Giuseppe, M. MPPT technique based on improved evaluation of photovoltaic parameters for uniformly irradiated photovoltaic array. *Electr. Power Syst. Res.* **2017**, *145*, 248–263. [[CrossRef](#)]
- Bendib, B.; Belmili, H.; Krim, F. A survey of the most used MPPT methods: Conventional and advanced algorithms applied for photovoltaic systems. *Renew. Sustain. Energy Rev.* **2015**, *45*, 637–648. [[CrossRef](#)]

28. Hammoudi, M.; Henao, C.; Agbossou, K.; Dubé, Y.; Doumbia, M. New multi-physics approach for modelling and design of alkaline electrolyzers. *Int. J. Hydrogen Energy* **2012**, *37*, 13895–13913. [[CrossRef](#)]
29. Ulleberg, Ø. Modeling of advanced alkaline electrolyzers: A system simulation approach. *Int. J. Hydrogen Energy* **2003**, *28*, 21–33. [[CrossRef](#)]
30. Jang, D.; Cho, H.-S.; Kang, S. Numerical modeling and analysis of the effect of pressure on the performance of an alkaline water electrolysis system. *Appl. Energy* **2021**, *287*, 116554. [[CrossRef](#)]
31. Sánchez, M.; Amores, E.; Rodríguez, L.; Clemente-Jul, C. Semi-empirical model and experimental validation for the performance evaluation of a 15 kW alkaline water electrolyzer. *Int. J. Hydrogen Energy* **2018**, *43*, 20332–20345. [[CrossRef](#)]
32. Roy, A.; Watson, S.; Infield, D. Comparison of electrical energy efficiency of atmospheric and high-pressure electrolyzers. *Int. J. Hydrogen Energy* **2006**, *31*, 1964–1979. [[CrossRef](#)]
33. Gül, M.; Akyüz, E. Hydrogen Generation from a Small-Scale Solar Photovoltaic Thermal (PV/T) Electrolyzer System: Numerical Model and Experimental Verification. *Energies* **2020**, *13*, 2997. [[CrossRef](#)]

Disclaimer/Publisher’s Note: The statements, opinions and data contained in all publications are solely those of the individual author(s) and contributor(s) and not of MDPI and/or the editor(s). MDPI and/or the editor(s) disclaim responsibility for any injury to people or property resulting from any ideas, methods, instructions or products referred to in the content.